

Article

Photocatalytic and Antimicrobial Activity of TiO₂ Films Deposited on Fiber-Cement Surfaces

Robson H. Rosa ^{1,2}, Ricardo S. Silva ³, Lucas L. Nascimento ⁴, Monica H. Okura ⁵, Antonio Otavio T. Patrocínio ^{4,*} and João A. Rossignolo ^{2,*}

¹ Instituto Federal de Educação, Ciência e Tecnologia do Triângulo Mineiro, Uberaba 38064-790, MG, Brazil

² Post-Graduation Program in Material Science and Engineering, Faculdade de Zootecnia e Engenharia de Alimentos, Universidade de São Paulo, Pirassununga 13635-900, SP, Brazil

³ Instituto de Ciências Exatas, Naturais e Educação, Universidade Federal do Triângulo Mineiro, Uberaba 38064-200, MG, Brazil

⁴ Laboratory of Photochemistry and Materials Science, Instituto de Química, Universidade Federal de Uberlândia, Uberlândia 38400-902, MG, Brazil

⁵ Instituto de Ciências Tecnológicas e Exatas, Universidade Federal do Triângulo Mineiro, Uberaba 38064-200, MG, Brazil

* Correspondence: otaviopatrocínio@ufu.br (A.O.T.P.); rossignolo@usp.br (J.A.R.)

Abstract: In this study, TiO₂ films were deposited via the doctor blade technique on fiber-cement surfaces. Two types of nanoparticles (TiO₂-P25 from Degussa and TiO₂-PC105 from Tronox) were used to produce films. Scanning electron microscopy (SEM) and atomic force microscopy (AFM) images revealed films with homogeneous and nanoparticulated morphology. The TiO₂ PC105 film presented a lower roughness parameter (RMS) in relation to that of the TiO₂ P25-based film. Both films exhibited high hydrophilicity when exposed to UV-A radiation (contact angle $\theta < 6^\circ$). The photocatalytic activity of the films was evaluated by standardized methylene blue dye degradation assays under UV-A irradiation (1.0 mW/cm²). The TiO₂-PC105 film showed a photonic efficiency of $\xi = 0.1\%$, while for the films obtained with TiO₂-P25, $\xi = 0.08\%$. The cement surface modified with the PC105 film was evaluated for antimicrobial activity through the use of multiple pathogens commonly found in hospitals. A considerably high efficiency was measured with visible light. Growth inhibition rates of $99.0\% \pm 0.2$, $99.1\% \pm 0.2$, $99.1\% \pm 0.2$, $97.5\% \pm 0.5$, $98.0\% \pm 0.5$ and $98.0\% \pm 0.5$ were found for *Staphylococcus aureus*, *Klebsiella* sp., *Escherichia coli*, *Rhizobium* sp., *Fusarium* sp. and *Penicillium* sp., respectively. The results show the self-cleaning ability and their potential use for protection, by preventing contamination of the fiber-cement surface and opening new possibilities for the use of this building material.

Keywords: self-cleaning films; functional surfaces; photocatalysis; antimicrobial activity



check for updates

Citation: Rosa, R.H.; Silva, R.S.; Nascimento, L.L.; Okura, M.H.; Patrocínio, A.O.T.; Rossignolo, J.A. Photocatalytic and Antimicrobial Activity of TiO₂ Films Deposited on Fiber-Cement Surfaces. *Catalysts* **2023**, *13*, 861. <https://doi.org/10.3390/catal13050861>

Academic Editor: Omid Akhavan

Received: 28 March 2023

Revised: 5 May 2023

Accepted: 6 May 2023

Published: 9 May 2023



Copyright: © 2023 by the authors. Licensee MDPI, Basel, Switzerland. This article is an open access article distributed under the terms and conditions of the Creative Commons Attribution (CC BY) license (<https://creativecommons.org/licenses/by/4.0/>).

1. Introduction

The increasing number of infections acquired in hospital environments has drawn attention in recent decades, especially due to the possibility of association with so-called “superbugs”, which proliferate due to the poor cleaning procedures used in such environments [1]. As a consequence, the search for new hygiene techniques for hospitals and other environments has intensified, such as the use of plasma, UV and photocatalytic systems [2–4]. Among these innovations, the possibility of applying photocatalytic films on the surfaces of different construction materials stands out. Such films have the potential to eliminate the fungi and bacteria that are deposited on them [3]. Among the various construction materials used globally, we highlight cementitious plates (fiber cement), which are used in the steel framing sealing system [5].

Among the microorganisms present in hospital environments, one is *Klebsiella pneumoniae*, a gram-negative, lactose-fermenting bacillus capable of producing serious infections in

patients with weakened immune systems, and which is frequently reported in the scientific literature for its adaptability and natural resistance to bactericidal agents [6]. Another opportunistic microorganism is the *Escherichia coli* bacterium, a gram-negative bacillus capable of causing colic, diarrhea, vomiting, renal failure, and in severe cases leads to the death of the patient [7]. The *Staphylococcus aureus* bacterium, also a very common microorganism in hospital environments, is a gram-positive bacillus that is capable of causing simple infections such as acne, boils, and cellulitis, as well as serious infections such as pneumonia, meningitis, endocarditis, sepsis, and others [8].

In addition to bacterial infections, the worldwide incidence of fungal infections has been increasing over the years, especially in patients undergoing solid organ transplantation, hematopoietic stem cells, and others [9,10]. In this scenario of increased fungicidal infections, the multidrug-resistant *Fusarium* sp. can be highlighted. Contamination from it may occur by the inhalation of airborne spores. In patients with compromised immune systems, it can cause respiratory, hepatic, renal, neurological, and other problems [9]. The fungus *Penicillium* sp., also grows in various environments (mainly in dark and airy places), in foods (such as bread, biscuits, and oranges), and is capable of producing mold and biodegradable organic matter, causing infections and poisoning in animals and humans [11].

TiO₂ is a stable semiconductor that has several technological applications [12], and its band gap energy is approximately 3.2 eV, therefore being activated by UV-A light, which leads to the formation of the so-called electron-hole pair (e⁻/h⁺) [13]. These charge carriers are very reactive and can recombine with each other or react with molecules adsorbed on the surface, such as water, oxygen, and (NO_x, SO₂). Under excitation, TiO₂ is capable of forming hydroxyl radicals and other reactive species which can degrade polluting molecules such as dyes [14], biomass-derived compounds [15], air pollutants [16], and inhibit microbial activity [17,18]. Thus, TiO₂ coatings have been extensively investigated for their antimicrobial activity, with potential promising applications resulting from their high physicochemical stability, non-toxicity, wide availability, and photocatalytic efficiency [19–21].

The application of TiO₂ films as hydrophilic and self-cleaning coatings has been extensively investigated, especially when deposited on glass surfaces [22–24], ceramic surfaces [25–28], and others. However, with regard to cement surfaces (fiber cement) studies in the scientific literature are scarce to date [29–32]. In this scenario, this study aimed to evaluate the photocatalytic activity of TiO₂ films deposited on cementitious surfaces (fiber cement) and their ability to inhibit the growth of various pathogens causing hospital infections and losses in the food industry.

2. Results and Discussion

2.1. Characterization of TiO₂ Powders

The crystalline phases of the TiO₂ powder samples (P25 Degussa and PC105 Tronox) were characterized by X-ray diffraction (XRD) analysis, as shown in Figure 1. The data confirm previous reports [33] and the manufacturer's information showing that TiO₂-PC105 are formed by an anatase (ICDD 21-1272) crystalline phase, while for TiO₂-P25, both anatase and rutile (ICDD 21-1276) crystalline phases were observed.

The average crystallite diameters were estimated using the Scherrer equation [34,35] at the anatase (101) and rutile (110) diffraction peaks. The percentages of crystalline phases were estimated using the Spurr & Myers equation [36]. The specific surface areas were obtained from an N₂ gas adsorption isotherm by the Brunauer-Emment-Teller (BET) method [37]. The results are shown in Table 1, and agree well with previous results for the TiO₂ nanoparticles [38,39].

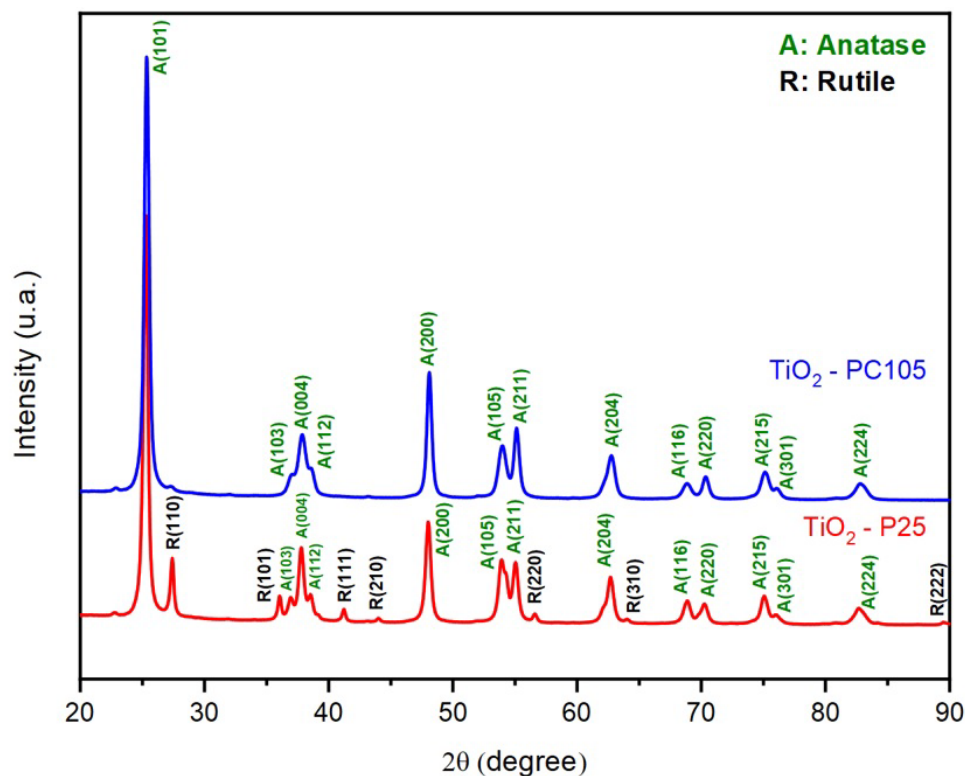


Figure 1. X-ray diffractogram of TiO₂ samples (P25 Degussa and PC105 Tronox).

Table 1. Characteristics of TiO₂ samples: specific surface area, average crystallite diameter, and percentage of phases.

Material	Specific Surface Area–(m ² /g)	Average Crystallite Diameter–(nm)		Percentage of Phases–(%)	
		Anatase	Rutile	Anatase	Rutile
TiO ₂ -P25	49.32	23.0	41.0	80.0	20.0
TiO ₂ -PC105	78.56	18.0	-	100.0	-

2.2. Characterization of TiO₂ Films

TiO₂ films were deposited on fiber cement surfaces by the Doctor Blade technique, as described in Section 4.2. Raman scattering is a technique that allows for the obtaining of information on the dynamics of the phonons characteristic of TiO₂, identifying whether the crystalline phase is anatase, rutile, or both [40]. The presence of the crystalline phases of TiO₂ in the films were analyzed by Raman vibrational spectroscopy, as shown in Figure 2. In the TiO₂-PC105 film, the presence of the anatase phase was verified through the active vibrational modes at 144 cm⁻¹, 399 cm⁻¹, 519 cm⁻¹, and 639 cm⁻¹, respectively [41,42]. In the TiO₂-P25 film, the presence of the anatase phase was verified in the active vibrational modes at 144 cm⁻¹, 399 cm⁻¹, 519 cm⁻¹, and 639 cm⁻¹, respectively [41–43], and rutile was verified at 443 cm⁻¹ and 610 cm⁻¹, respectively [42,43]. As expected, the methodology employed for thin film deposition did not lead to changes in the TiO₂ particles. From the Raman data, there is no sign that any component of the fiber-cement substrate chemically reacts with the photocatalyst.

Scanning electron microscopy images, shown in Figure 3a, showed that both films are homogeneous and formed by aggregates of nanoparticulates. The TiO₂-PC105 film presents itself as a cluster of overlapping particles with an uneven distribution, completely covering the substrate. The film formed by TiO₂-P25 shows very homogeneous and densely packed

particles. However, some cracks were observed on the surface of the film, as also reported in other studies [44–46].

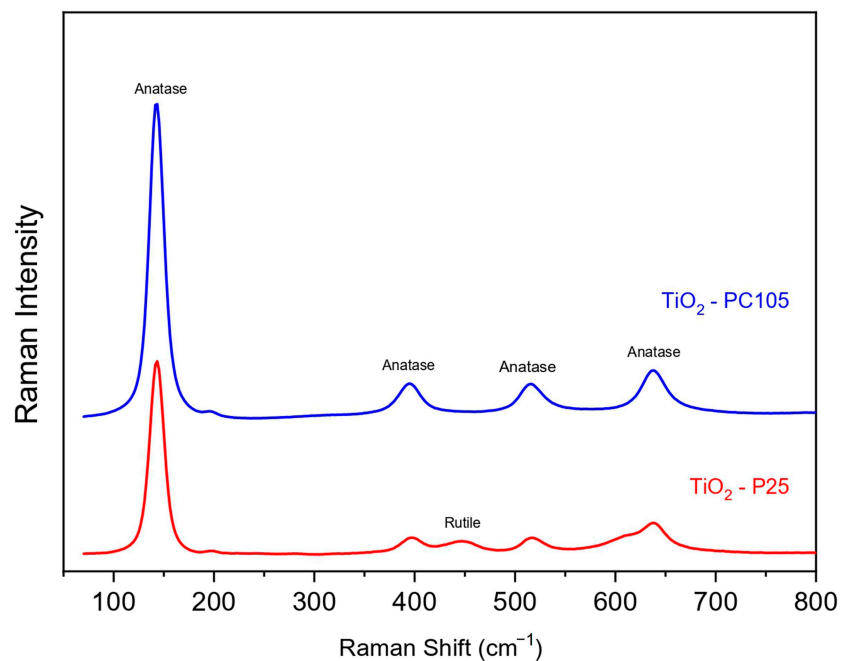


Figure 2. Raman spectrum of TiO₂ films (Evonik P25 and Tronox PC105).

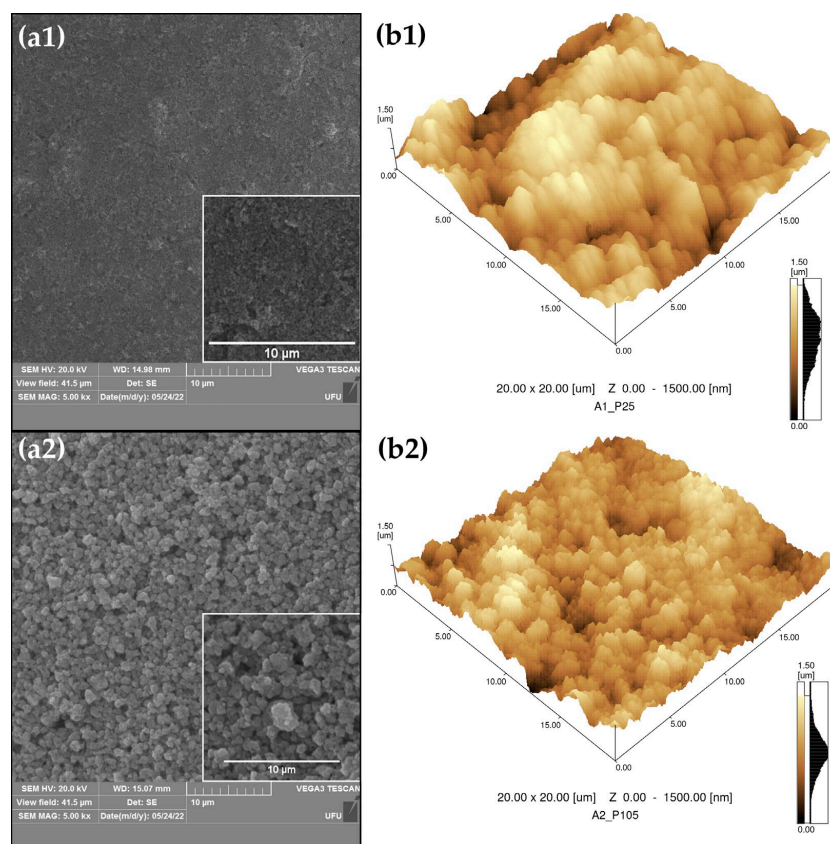


Figure 3. (a) Scanning Electron Microscopy Images: (a1) TiO₂ Film-P25; (a2) TiO₂ Film-PC105. (b) Atomic force microscopy images: (b1) TiO₂ Film-P25; (b2) TiO₂ Film-PC105.

Atomic force microscopy images, as shown in Figure 3b, showed that both films were nanoparticulated and that the surfaces were relatively rough. The TiO₂-P25 film presented a roughness parameter (RMS = 264 nm) slightly higher than that for TiO₂-PC105 film (RMS = 217 nm).

The wettability of the films was evaluated through contact angle measurements [47] in triplicate, Figure 4. The fiber cement surface covered with acrylic paint, used as a reference, presented a contact angle ($\theta = 65 \pm 3$ degrees), characteristic of a hydrophilic surface, whereas the coverage with TiO₂ films lead to contact angles of 9 ± 1 degree before irradiation with UV-A light source, and <6 degree after irradiation with UV-A light source. These values are characteristic of super hydrophilic surfaces and are compared to the literature in Table 2.

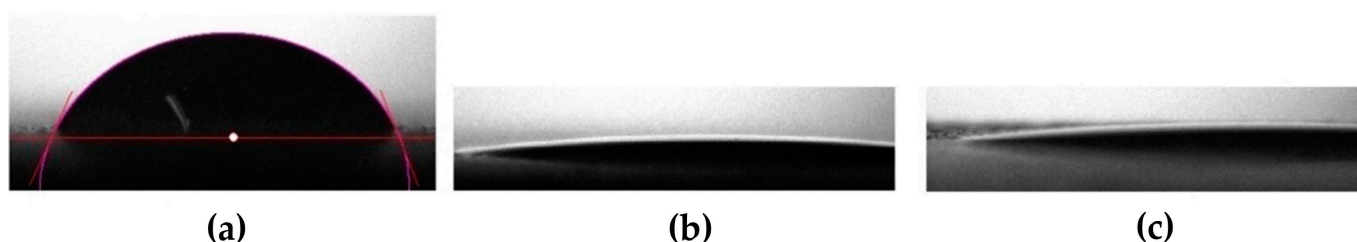


Figure 4. Contact angle images after UV-A irradiation: (a) fiber cement plate with acrylic paint, (b) TiO₂ film-P25, (c) TiO₂-PC105.

Table 2. Data of contact angle measurements of TiO₂ films before and after UV-A irradiation.

Substrate	Contact Angle		Reference
	Before UV-A Irradiation	After UV-A Irradiation	
Plate with acrylic paint	65 ± 3	65 ± 3	–
TiO ₂ -P25	9 ± 1	<6	–
TiO ₂ -PC105	9 ± 1	<6	–
Orthodontic Resin coated with TiO ₂	80 ± 5	34 ± 1	[48]
Self-assembled TiO ₂ thin films on FTO glass	12 ± 2	<5	[47]
TiO ₂ thin films on FTO	70 ± 5	<10	[49]

The photocatalytic properties of the films were evaluated by the degradation of the methylene blue dye under UV-A irradiation after 60 min equilibration in the dark. Degradation tests were performed in triplicate. Control photoirradiation experiments employing the MB solution without any photocatalyst as well as the fiber-cement substrate itself that were carried out lead to negligible ($<2\%$) variations on the MB concentration within 240 min. Both films exhibited photocatalytic activity, and the concentration of methylene blue decreased as a result of its decomposition in the presence of TiO₂ [50], as illustrated in Figure 5a. Differences in photocatalytic activity are related to several factors, including the size of TiO₂ nanoparticles [51–53], the composition of crystalline phases [54,55], the specific surface area [51,53,56]; and film morphology [57–59].

The degradation rate constants (k) were obtained considering the degradation reaction as a pseudo first-order kinetic, and the light photons as a constant concentration reagent [50,60,61]. The degradation rate was estimated with Equation (1).

$$v = \frac{k \times (MB)_0 \times V_s}{60} \quad (1)$$

where (k) is the degradation rate constant, in (min^{-1}), (MB) the initial concentration of the methylene blue solution in (mol/L), and (V_s) the volume of the methylene blue solution, in (L). The photonic efficiency (ξ) was estimated using Equation (2), where (I_0) the intensity of the UV-A source, in (Einstein/s). The data found are shown in Table 3.

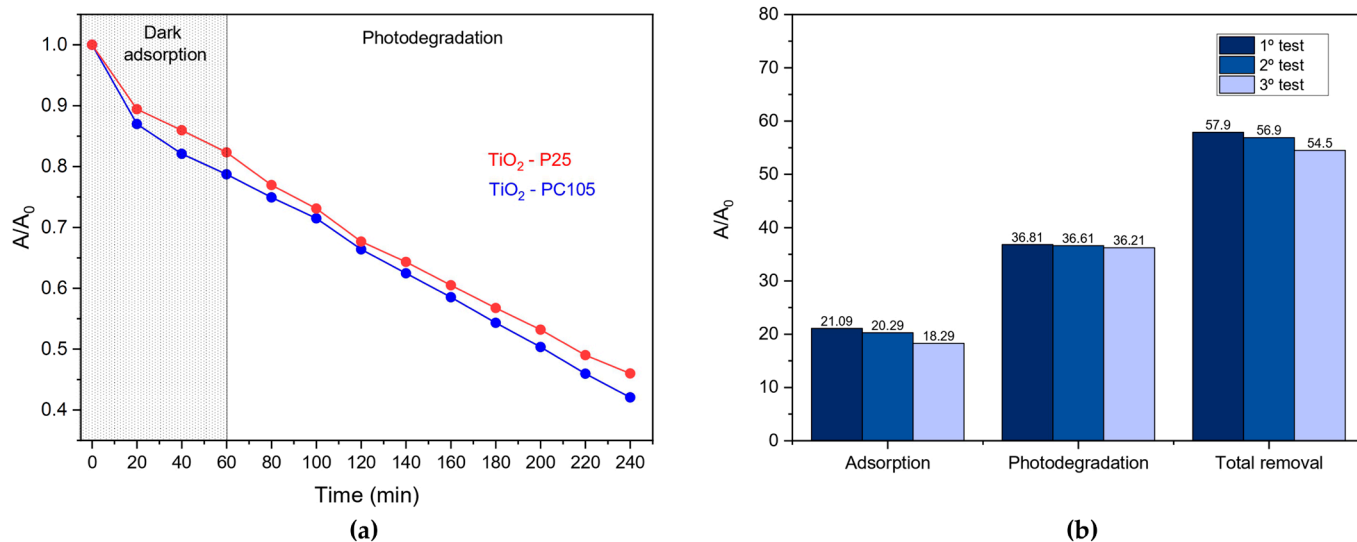


Figure 5. (a) Graph A/A_0 versus time for TiO_2 films (Evonik P25 and Tronox PC105); (b) Durability of TiO_2 film-PC105 via a consecutive dye degradation test.

$$\xi = \left(\frac{v}{I_0} \right) \times 100 \quad (2)$$

Table 3. Data obtained from methylene blue dye degradation tests.

Parameter	Film	
	$\text{TiO}_2\text{-P25}$	$\text{TiO}_2\text{-PC105}$
Velocity constant- k_{obs} (min^{-1})	3.21×10^{-3}	3.48×10^{-3}
Degradation rate- v (mol/s)	2.14×10^{-11}	2.32×10^{-11}
Source Intensity- I_0 (Einstein/s)	2.45×10^{-8}	2.45×10^{-8}
Adsorption in the dark-(%)	17.7 ± 0.5	21.3 ± 0.5
Photodegradation after 3 h irradiation-(%)	36.3 ± 0.5	36.6 ± 0.5
Total removal-(%)	54.0 ± 0.5	57.9 ± 0.5
Photonic efficiency- ξ (%)	0.08	0.1

The adsorption of the films in the dark was evaluated from the reduction in absorption values at 663 nm of the methylene blue solution. The $\text{TiO}_2\text{-PC105}$ film showed a slightly higher percentage of adsorption in the dark compared to the $\text{TiO}_2\text{-P25}$ film. This small difference may have occurred due to the specific surface area differences of the TiO_2 nanoparticles (P25 Degussa and PC105 Tronox), see Table 1 [51,53]. The photodegradation of the methylene blue dye was analyzed for a period of 180 minutes, evaluating the decrease in the absorption values at 663 nm every 20 min. The photodegradation performance was very similar for both films, despite the difference in the morphology and structure of the materials, which leads us to infer that photocatalytic degradation of MB is being limited by charge-transfer kinetics rather than surface area. Lastly, the $\text{TiO}_2\text{-PC105}$ film showed better photonic efficiency, and had its durability evaluated through three consecutive methylene

blue dye degradation tests. The tests were performed every 24 h, always with the same TiO₂ film, but with new concentrations of methylene blue, following the methodology described in item 3.4. The percentage of photodegradation remained practically constant throughout the tests, as shown in Figure 5b. However, there was a slight decrease in the percentage of adsorption in the dark, probably due to the agitation of the solution every 20 min, with a consequent slight decrease of around 3.4% in the percentage of total dye removal, which was mainly due to the deposition of carbon residues onto the surface of the film.

2.3. Antimicrobial Evaluation

Studies indicate that oxidative radicals generated during TiO₂ photocatalysis are capable of decomposing organic molecules, and can interact with living microorganisms such as bacteria, fungi, algae, and others, causing damage to cell membranes and consequent cell death [20,62–65]. In 2012, Liu & Chang [66] suggested that the antibacterial mechanism of TiO₂ begins with the damage to the cell membrane, followed by the leakage of the internal components of the cell, and finally the oxidation of cellular debris, thereby causing the death of the bacterium [66]. In this study, the bactericidal activity of the TiO₂-PC105 film was evaluated by inhibiting the growth of bacteria (*Staphylococcus aureus*, *Klebsiella* sp., *Escherichia coli*) based on the number of colonies formed on a nutrient agar plate [67], comparing the contact time of the film with the inoculum for 15 min and 60 min. The films with the different inoculum were exposed to a fluorescent lamp typically found in indoor environments. The percentage of bacteria growth inhibition was calculated by taking the number of microorganisms found in the absence of TiO₂ films as the basis, and the tests were performed in triplicate. In the assays with a contact time of 15 min, the efficiency (inhibition of bacterial growth) was above (99.0% ± 0.20), and with a time of 60 min the efficiency was (99.90% ± 0.02) for the three strains of bacteria, which can be found on the surfaces of hospital environments [68–70]. The results obtained showed a high efficiency of the TiO₂ film on the Gram-positive and Gram-negative strains of the bacteria, when excited with indoor light. The results are shown in Figure 6a.

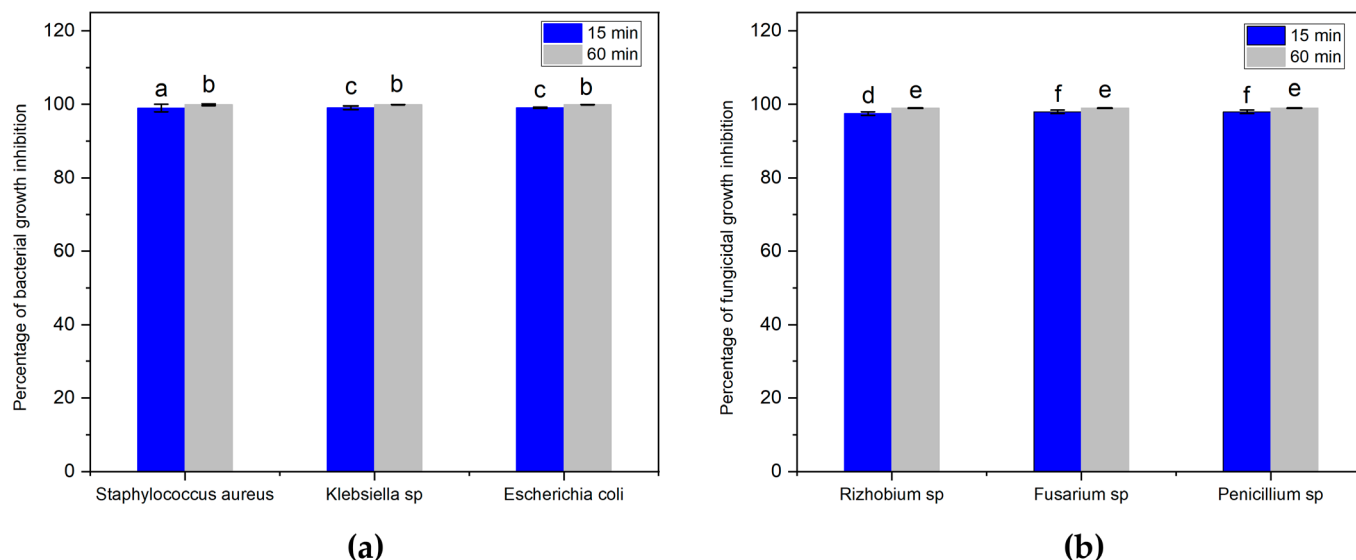


Figure 6. Bactericidal (a) and fungicidal (b) activities of PC105 TiO₂ film. The different letters indicate significantly different mean values according to the Tukey HSD test ($p < 0.05$; $n = 3$).

The fungicidal activity of the TiO₂-PC105 film was evaluated by inhibiting the growth of fungi (*Rhizobium* sp., *Fusarium* sp., *Penicillium* sp.) based on the number of colonies formed in Potato Dextrose Agar (PDA), comparing the contact time of the film with the inoculum for 15 min and 60 min. The percentage of fungi growth inhibition in the absence

of TiO₂ films was normalized to 0%, and the tests were performed in triplicate. In the assays with contact times of 15 min, the efficiency (inhibition of fungicidal growth) was above (97.5% ± 0.5), and with a time of 60 min the efficiency was (99.0% ± 0.1) for the three fungal lines, which can be found in the environment of food industries [71,72]. The results obtained showed the high efficiency of the TiO₂ film on the three fungi evaluated when excited with indoor light. The results are shown in Figure 6b.

Existing studies in the literature evaluating the antimicrobial activity of TiO₂ films with light sources (UV-A, visible light, and dark), substrates (glass, stainless steel, ceramic flooring, and cementitious composite), and pathogenic microorganisms (bacteria, fungi, and algae) are shown in Table 4. The current study includes a robust investigation with multiple pathogens (bacteria and fungi) on the cement surface (fibercement), therefore being innovative in nature, and led to excellent results when compared to the results reported for TiO₂ films in different substrates.

Table 4. Photocatalytic performance of different TiO₂-films deposited over different substrates towards the inhibition of microorganism growth.

References	Light Source	Substrate	Microorganisms	Main Results
[73]	Visible light	Floor ceramic tiles	<i>Escherichia coli</i> , <i>Staphylococcus aureus</i> ,	<i>S. aureus</i> ATCC 6538 and <i>E. coli</i> ATCC 259 were reduced by 99 and 95%, respectively
[74]	UV-A/Dark	Glass	<i>Escherichia coli</i> , <i>Staphylococcus aureus</i>	>2.8 log decrease in <i>E. coli</i> and >2.5 log decrease in <i>S. aureus</i> viable cell counts after 4 h
[75]	UV-A	Cementitious composite	<i>Penicillium notatum</i> , <i>Aspergillus niger</i>	50.4% <i>Penicillium notatum</i> inhibition after 3 days of exposure
[76]	UV-A/Dark	Glass	<i>Escherichia coli</i> , <i>Staphylococcus aureus</i> , <i>Pseudomonas aeruginosa</i>	Near 100% killing of <i>Pseudomonas aeruginosa</i> over 24 h of irradiation
[77]	UV-A	Glass	<i>Escherichia coli</i> , Bacteriophage T4	Near 100% killing of bacteriophage T4 after 2 h of irradiation
[20]	–	Stainless steel	<i>Escherichia coli</i> , <i>Staphylococcus aureus</i> ,	>5log reduction of <i>Staphylococcus aureus</i> after 40 h of exposure
[78]	UV-A	Stainless steel	<i>Escherichia coli</i>	Near 100% killing of <i>E. Coli</i> in less than 3 h

3. Conclusions

The Doctor Blade deposition technique was successfully applied in the production of TiO₂ self-cleaning films on fiber cement surfaces. Both films exhibited a homogeneous and nanoparticulated morphology. The wettability tests showed that the surfaces with the films are superhydrophilic, even in the absence of UV-A irradiation. The antimicrobial results showed a high efficiency (inhibition of pathogen growth) of the TiO₂-PC105 film against the Gram-positive and Gram-negative strains of bacteria, and also against fungi. The results were promising and showed that the films can be applied on fiber cement surfaces as protection, avoiding contamination, especially in hospital environments and in the food industry.

4. Materials and Methods

4.1. Characterization of the Raw Material

The crystal structure and phases of TiO₂ were investigated using an X-ray diffractometer (XRD). XRD patterns were obtained using a Rigaku MiniFlex 600 diffractometer using CuK α radiation ($\lambda = 1.5406 \text{ \AA}$), operating with a voltage of 40 kV and electrical current

of 15 mA, in a range of 10 to 90° in 2θ mode, with a scanning speed of 0.5°/min. The Scherrer method [34,35] was employed to estimate the average size of the crystallite, using the width of the half height of the peak of greater intensity (101), in the anatase phase of TiO₂. The percentages of anatase and rutile crystalline phases were estimated using the Spurr & Myers method [36]. The specific surface area (SEA) was measured from the adsorption/desorption of gaseous N₂ by the Brunauer-Emmett-Teller (BET) method [37]. The tests were conducted on a Belsorp Max Microtrac MRB model. The samples were pretreated under gaseous N₂ flow for 24 h at 110 °C in order to remove adsorbed gases and water. In the tests, approximately 0.18 g of sample and liquid N₂ were used to maintain the temperature of 77 K during the analysis.

4.2. The Production and Deposition of TiO₂ Films

All raw materials were used without further purification. An amount of 1.0 g of TiO₂ was added into a previously homogenized solution containing 12.0 mL of ethyl alcohol (99.5%), 0.4 mL of glacial acetic acid (99.9%), and 0.4 mL of Tween 20, forming a homogeneous paste. Next, the paste was placed in an ultrasonic bath for 30 min at room temperature (~25 °C). The paste was then placed under constant magnetic stirring for 24 h. TiO₂ films were deposited by the doctor blade method on fiber cement plates coated with commercial acrylic paint (5.0 × 5.0 × 1.0 cm) that was previously subjected to a cleaning process. After deposition, the films were treated at 100 °C for 1 h.

4.3. Characterization of TiO₂ Films

The structural analysis of the films was investigated using Raman vibrational spectra. The spectra were obtained using a Horiba brand LabRAM HR Revolution spectrometer equipped with an excitation laser at 532 nm and a diffraction network with 600 grooves mm⁻¹, with a scanning speed of 43 cm/s. The morphology of the films was evaluated by scanning electron microscopy (SEM) using a TESCAN model Vega 3 scanning electron microscope equipped with a secondary electron detector. The images were obtained with 20 kV of acceleration voltage. The topography of the films was evaluated by atomic force microscopy (AFM) using a Shimadzu model SPM-9600 microscope, in contact mode, with a scan rate of 1.0 Hz, with the aid of an Olympuz OMCL-TR800PSA-1 model cantilever. The wettability of the films was evaluated from measurements of the contact angle using the sessile drop method before and after 30 min of UV-A irradiation. To perform the tests, we used a Theta Lite optical tensiometer from Attension coupled to a OneAttension micro CCD camera.

4.4. Photocatalytic Properties

The photocatalytic activity of the films was investigated through the methylene blue dye degradation tests, following the setup reported in the technical standard ISO 10678 [79]. To carry out the tests, a glass cylinder of 3.4 cm diameter was fixed on the fiber cement plate (using silicon sealant). In this system, the plate-cylinder was added to the aqueous solution of methylene blue dye, with an initial concentration of 2×10^{-5} mol/L, until reaching a height of 2.2 cm, as shown in Figure 7. Different from the recommendation of ISO 10678, the films were allowed to be in contact with the methylene blue solution for 60 min prior to irradiation. Within this time, the MB adsorption by the two different films was approximately 20%.

The tests were performed using three Philips TL 8 W lamps that emit UV-A radiation in the region between 300–390 nm with a maximum intensity at 365 nm, coupled to a support with height regulation. The height of the lamps was adjusted so that the radiated power was 1.0 mW/cm². The power measurements were performed using an Ocean Optics USB2000+ spectrometer equipped with an optical fiber and irradiance probe. Initially, the samples were subjected to 1 h of adsorption in the dark, and they were subsequently exposed to UV-A radiation for 3 h. Throughout the process, the suspensions were kept at constant temperature (~25 °C), and were manually agitated every 20 min. The variation in

the concentration of methylene blue dye as a function of irradiation time was evaluated by measuring the absorbance of the solution at 664 nm every 20 min, with the aid of a GTA-96S Global Analyzer UV-VIS spectrophotometer.

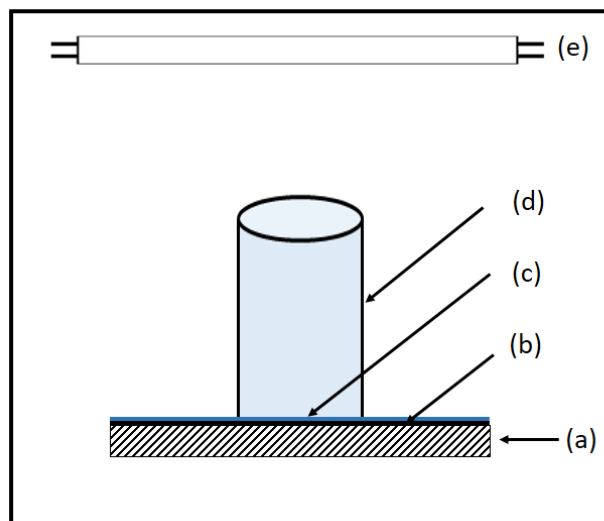


Figure 7. Illustration of the dye degradation test device with UV-A light, where: (a) fiber cement plate, (b) acrylic paint layer, (c) TiO₂ film, (d) cylinder with the dye solution, (e) UV-A light source.

4.5. Antimicrobial Tests

In order to evaluate the antimicrobial activity of TiO₂ films, strains of bacteria (*Staphylococcus aureus*, *Klebsiella pneumoniae*, *Escherichia coli*) and fungi (*Rhizobium* sp., *Fusarium* sp., *Penicillium* sp.) were used. TiO₂-PC105 films showed better photonic efficiency results and total removal of methylene blue dye compared to TiO₂-P25, as shown in Table 3. They were deposited on previously cleaned substrates using the doctor blade method, in an ultrasonic bath for 10 min at room temperature (~25 °C) with 70% ethyl alcohol, and then dried in an oven at 60 °C for 1 h. The films have a thickness of 6×10^{-3} cm and an area of 18.0 cm².

For the preparation of the inoculum of the bacteria (initial count), the colonies of bacteria were collected and placed in 9 mL of sterile saline (0.9%). This procedure generated an inoculum of 1×10^6 CFU/mL, and this value was confirmed by the plating of 0.01 mL of the suspension in nutrient agar (NA), and the subsequent counting of the colonies of bacteria after incubation of the plates for a period of 24 to 48 h at a temperature of 37 °C. For the bactericidal tests, the substrates with the TiO₂ film were initially exposed to UV-A radiation, with a power of 1 mW/cm², for 30 min, after which they were placed in a 50 mL Falcon tube, after which 45 mL of sterile saline water (0.1%) was added to the tube. An amount of 1 mL of the inoculum of the bacteria was added, stirring in the vortex for 1 min. After homogenization, the inoculum remained in contact with TiO₂ film for 15 min and 60 min under indoor irradiation provided by a fluorescent lamp. Subsequently, 1 mL of this sample was inoculated in a plate containing NA, and the plates were then incubated at a temperature of 37 °C for a period of 24 to 48 h. The counting was performed after this period.

For the preparation of the fungal inoculum (initial count), the fungal colonies were collected and placed in 9 mL of sterile saline (0.9%). This procedure generated an inoculum of 1×10^6 CFU/mL, and this value was confirmed by the plating of 0.01 mL of the suspension in Potato Dextrose Agar (PDA) and the subsequent counting of the fungal colonies after incubation of the plates for a period of 7 to 10 days at a temperature of 28 °C. For the tests, the glass slides with the TiO₂ film were initially exposed to UV-A radiation, with a power of 1 mW/cm², for 30 min, after which they were placed in a 50 mL Falcon tube, and 45 mL of sterile saline water (0.1%) was then added to the tube. An amount of 1 mL of the fungus inoculum was added, stirring in the vortex for 1 min. After

homogenization, the inoculum remained in contact with TiO₂ film for 15 min and 60 min under indoor irradiation provided by a fluorescent lamp. Subsequently, 1 mL of this sample was inoculated in a plate containing PDA. The plates were then incubated at a temperature of 28 °C for a period of 5 days. The counting was performed after this period.

All inhibition growth percentages were calculated by taking the amount of the microorganisms observed for pristine substrates submitted to the same procedure as those containing the TiO₂ films.

Author Contributions: All authors contributed to the study conception and design. Material preparation, data collection, and analysis were performed by R.H.R., R.S.S. and L.L.N. Conceptualization, methodology, formal analysis, validation, resources, data curation, writing—review and editing, visualization, supervision, project administration, and funding acquisition were performed by J.A.R., M.H.O. and A.O.T.P. The first draft of the manuscript was written by R.H.R., and all authors commented on previous versions of the manuscript. All authors have read and agreed to the published version of the manuscript.

Funding: This work was supported by FAPEMIG (Fundação de Amparo à Pesquisa do Estado de Minas Gerais), CAPES (Coordenação de Aperfeiçoamento de Pessoal de Nível Superior), and CNPq (Conselho Nacional de Desenvolvimento Científico e Tecnológico).

Data Availability Statement: The data presented in this study are available on request from the corresponding author.

Acknowledgments: The authors gratefully acknowledge Brazilian funding agencies (CNPq, CAPES, and FAPEMIG) for financial support. The authors are also thankful to the Institute of Physics (INFIS-UFU) multiuser lab and Institute of Exact and technological Sciences (ICTE-UFTM).

Conflicts of Interest: The authors declare no conflict of interest.

References

1. Thomas, R.E.; Thomas, B.C.; Conly, J.; Lorenzetti, D. Cleaning and disinfecting surfaces in hospitals and long-term care facilities for reducing hospital- and facility-acquired bacterial and viral infections: A systematic review. *J. Hosp. Infect.* **2022**, *122*, 9–16. [[CrossRef](#)] [[PubMed](#)]
2. Rudhart, S.A.; Gunther, F.; Dapper, L.; Stuck, B.A.; Hoch, S. UV-C Light-Based Surface Disinfection: Analysis of Its Virucidal Efficacy Using a Bacteriophage Model. *Int. J. Environ. Res. Public Health* **2022**, *19*, 3246. [[CrossRef](#)] [[PubMed](#)]
3. Margarucci, L.M.; Spica, V.R.; Protano, C.; Gianfranceschi, G.; Giuliano, M.; Di Onofrio, V.; Mucci, N.; Valeriani, F.; Vitali, M.; Romano, F. Potential antimicrobial effects of photocatalytic nanotechnologies in hospital setting. *Ann. Ig. Med. Prev. Comunita* **2019**, *31*, 461–473. [[CrossRef](#)]
4. Mitra, A.; Morfill, G.E.; Shimizu, T.; Steffes, B.; Isbary, G.; Schmidt, H.U.; Li, Y.F.; Zimmermann, J.L. Applications in plasma medicine: A SWOT approach. *Compos. Interfaces* **2012**, *19*, 231–239. [[CrossRef](#)]
5. Soltan, D.G.; Das Neves, P.; Olvera, A.; Savastano Junior, H.; Li, V.C. Introducing a curauá fiber reinforced cement-based composite with strain-hardening behavior. *Ind. Crops Prod.* **2017**, *103*, 1–12. [[CrossRef](#)]
6. Baroud, M.; Dandache, I.; Araj, G.F.; Wakim, R.; Kanj, S.; Kanafani, Z.; Khairallah, M.; Sabra, A.; Shehab, M.; Dbaibo, G.; et al. As underlying mechanisms of carbapenem resistance in extended-spectrum β -lactamase-producing *Klebsiella pneumoniae* and *Escherichia coli* isolates at a tertiary care centre in Lebanon: Role of OXA-48 and NDM-1 carbapenemases. *Int. J. Antimicrob. Agents* **2013**, *41*, 75–79. [[CrossRef](#)]
7. Ozturk, I.; Tunçel, A.; Ince, M.; Ocakoglu, K.; Hoşgör-limoncu, M.; Yurt, F. Antibacterial properties of subphthalocyanine and subphthalocyanine-TiO₂ nanoparticles on *Staphylococcus aureus* and *Escherichia coli*. *J. Porphyr. Phthalocyanines* **2018**, *22*, 1099–1105. [[CrossRef](#)]
8. Jiang, X.; Lv, B.; Wang, Y.; Shen, Q.; Wang, X. Bactericidal mechanisms and effector targets of TiO₂ and Ag-TiO₂ against *Staphylococcus aureus*. *J. Med. Microbiol.* **2017**, *66*, 440–446. [[CrossRef](#)]
9. Lockhart, S.R.; Guarner, J. Emerging and reemerging fungal infections. *Semin. Diagn. Pathol.* **2019**, *36*, 177–181. [[CrossRef](#)]
10. Richardson, M.; Lass-flor, C. Changing epidemiology of systemic fungal infections. *Clin. Microbiol. Infect.* **2008**, *14*, 5–24. [[CrossRef](#)]
11. Kirk, P.M.; Cannon, P.F.; Minter, D.W.; Stalpers, J.A. *Ainsworth and Bisby's Dictionary of the Fungi*, 10th ed.; CABI: Wallingford, UK, 2008. [[CrossRef](#)]
12. Padmanabhan, N.T.; John, H. Titanium dioxide based self-cleaning smart surfaces: A short review. *J. Environ. Chem. Eng.* **2020**, *8*, 104211. [[CrossRef](#)]
13. Fujishima, A.; Rao, T.N.; Tryk, D.A. Titanium dioxide photocatalysis. *J. Photochem. Photobiol. C Photochem. Rev.* **2000**, *1*, 1–21. [[CrossRef](#)]

14. Reza, K.M.; Kurny, A.; Gulshan, F. Parameters affecting the photocatalytic degradation of dyes using TiO₂: A review. *Appl. Water Sci.* **2017**, *7*, 1569–1578. [[CrossRef](#)]
15. Colmenares, J.C.; Luque, R. Heterogeneous photocatalytic nanomaterials: Prospects and challenges in selective transformations of biomass-derived compounds. *Chem. Soc. Rev.* **2014**, *43*, 765–778. [[CrossRef](#)]
16. Kotzias, D.; Binas, V.; Kiriakidis, G. Smart Surfaces: Heterogeneous Photo-Catalysis on TiO₂ Based Coatings for De-pollution Purposes in Indoor and Outdoor Environments. *Top. Catal.* **2020**, *63*, 875–881. [[CrossRef](#)]
17. Kumaravel, V.; Nair, K.M.; Mathew, S.; Bartlett, J.; Kennedy, J.E.; Manning, H.G.; Whelan, B.J.; Leyland, N.S.; Pillai, S.C. Antimicrobial TiO₂ nanocomposite coatings for surfaces, dental and orthopaedic implants. *Chem. Eng. J.* **2021**, *416*, 129071. [[CrossRef](#)]
18. Amézaga-Madrid, P.; Nevárez-Moorillón, G.V.; Orrantia-Borunda, E.; Miki-Yoshida, M. Photoinduced bactericidal activity against *Pseudomonas aeruginosa* by TiO₂ based thin films. *FEMS Microbiol. Lett.* **2002**, *211*, 183–188. [[CrossRef](#)]
19. Prakash, J.; Cho, J.; Mishra, Y.K. Photocatalytic TiO₂ nanomaterials as potential antimicrobial and antiviral agents: Scope against blocking the SARS-COV-2 spread. *Micro Nano Eng.* **2022**, *14*, 100100. [[CrossRef](#)]
20. Chung, C.-J.; Lin, H.-I.; Tsou, H.-K.; Shi, Z.-Y.; He, J.-L. An antimicrobial TiO₂ coating for reducing hospital-acquired infection. *J. Biomed. Mater. Res. Part B Appl. Biomater.* **2008**, *85*, 220–224. [[CrossRef](#)]
21. FU, G.; Vary, P.S.; Lin, C.T. Anatase TiO₂ Nanocomposites for Antimicrobial Coatings. *J. Phys. Chem. B* **2005**, *109*, 8889–8898. [[CrossRef](#)]
22. Lukong, V.T.; Mouchou, R.T.; Enebe, G.C.; Ukoba, K.; Jen, T.C. Deposition and characterization of self-cleaning TiO₂ thin films for photovoltaic application. *Mater. Today: Proc.* **2022**, *62*, S63–S72. [[CrossRef](#)]
23. Xi, R.; Wang, Y.; Wang, X.; Lv, J.; Li, X.; Li, T.; Zhang, X.; Du, X. Ultrafine nano-TiO₂ loaded on dendritic porous silica nanoparticles for robust transparent antifogging self-cleaning nanocoatings. *Ceram. Int.* **2020**, *46*, 23651–23661. [[CrossRef](#)]
24. Xi, B.; Verma, L.K.; Li, J.; Bhatia, C.S.; Danner, A.J.; Yang, H.; Zeng, H.C. TiO₂ Thin Films Prepared Via Adsorptive Self-Assembly for Self-Cleaning Applications. *ACS Appl. Mater. Interfaces* **2012**, *4*, 1093–1102. [[CrossRef](#)]
25. Wu, H. Nanometer TiO₂ Film-Based Solar Thin Film Manufacturing Technology and Performance Research. *Adv. Mater. Sci. Eng.* **2022**, *2022*, 8328378. [[CrossRef](#)]
26. Ducman, V.; Petrovic, V.; Skapin, S.D. Photo-catalytic efficiency of laboratory made and commercially available ceramic building products. *Ceram. Int.* **2013**, *39*, 2981–2987. [[CrossRef](#)]
27. Zhang, P.; Tian, J.; Xu, R.; Ma, G. Hydrophilicity, photocatalytic activity and stability of tetraethyl orthosilicate modified TiO₂ film on glazed ceramic surface. *Appl. Surf. Sci.* **2013**, *266*, 141–147. [[CrossRef](#)]
28. Kim, M.-S.; Liu, G.; Cho, H.-K.; Kim, B.-W. Application of a hybrid system comprising carbon-doped TiO₂ film and a ceramic media-packed biofilter for enhanced removal of gaseous styrene. *J. Hazard. Mater.* **2011**, *190*, 537–543. [[CrossRef](#)]
29. Custódia, P.; Lied, E.B.; Da Silva, A.V.; Frare, L.M.; Bittencourt, P.R.S.; De Oliveira Basso, R.L.; De Oliveira Tavares, F.; Ferandin Honório, J.; Trevisan, A.P. TiO₂ coated fiber cement composites: Effect of the load of TiO₂ particles on photocatalytic degradation of H₂S. *Constr. Build. Mater.* **2020**, *262*, 120379. [[CrossRef](#)]
30. Wang, J.; Lu, C.H.; Xiong, J. Self-Cleaning and Depollution of Fiber Reinforced Cement Materials Modified by Neutral TiO₂/SiO₂ Hydrosol Photoactive Coatings. *Appl. Surf. Sci.* **2014**, *298*, 19–25. [[CrossRef](#)]
31. Guo, X.; Rao, L.; Wang, P.; Wang, C.; Ao, Y.; Jiang, T.; Wang, W. Photocatalytic Properties of P25-Doped TiO₂ Composite Film Synthesized via Sol-Gel Method on Cement Substrate. *J. Environ. Sci.* **2018**, *66*, 71–80. [[CrossRef](#)]
32. Yuenyongsuwan, J.; O’Rear, E.A.; Pongprayoon, T. Admicellar Polymerization of a Co-Fluoropolymer Ultrathin Film on TiO₂ Nanoparticles for Use as a Photocatalytic Cement. *Surf. Interfaces* **2021**, *25*, 101172. [[CrossRef](#)]
33. Dantas, S.R.A.; Lima, F.J.N.; Romano, R.C.O.; Pileggi, R.; Loh, K. Evaluation of rheological properties of mortar with TiO₂ addition. *Ambiente Construído* **2021**, *21*, 7–21. [[CrossRef](#)]
34. Patterson, A.L. X-Ray Diffraction Procedures for Polycrystalline and Amorphous Materials. *J. Am. Chem. Soc.* **1955**, *77*, 2030–2031. [[CrossRef](#)]
35. Neto, W.P.F.; Silvério, H.A.; Dantas, N.O.; Pasquini, D. Extraction and characterization of cellulose nanocrystals from agro-industrial residue—Soy hulls. *Ind. Crops Prod.* **2013**, *42*, 480–488. [[CrossRef](#)]
36. Spurr, R.A.; Myers, H. Quantitative Analysis of Anatase-Rutile Mixtures with an X-Ray Diffractometer. *Anal. Chem.* **1957**, *29*, 760–762. [[CrossRef](#)]
37. Brunauer, S.; Emmett, P.H.; Teller, E. Adsorption of Gases in Multimolecular Layers. *J. Am. Chem. Soc.* **1938**, *60*, 1938. [[CrossRef](#)]
38. Folli, A.; Pochard, I.; Nonat, A.; Jakobsen, U.H.; Shepherd, A.M.; Macphee, D.E. Engineering Photocatalytic Cements: Understanding TiO₂ Surface Chemistry to Control and Modulate Photocatalytic Performances. *J. Am. Ceram. Soc.* **2010**, *93*, 3360–3369. [[CrossRef](#)]
39. Uddin, M.J.; Cesano, F.; Chowdhury, A.R.; Trad, T.; Cravanzola, S.; Martra, G.; Mino, L.; Zecchina, A.; Scarano, D. Surface Structure and Phase Composition of TiO₂ P25 Particles After Thermal Treatments and HF Etching. *Front. Mater.* **2020**, *7*, 192. [[CrossRef](#)]
40. Challagulla, S.; Tarafder, K.; Ganesan, R.; Roy, S. Structure sensitive photocatalytic reduction of nitroarenes over TiO₂. *Sci. Rep.* **2017**, *7*, 8783. [[CrossRef](#)]
41. Cho, H.-W.; Liao, K.-L.; Yang, J.-A.; Wu, J.-J. Revelation of rutile phase by Raman scattering for enhanced photoelectrochemical performance of hydrothermally-grown anatase TiO₂ film. *Appl. Surf. Sci.* **2018**, *440*, 125–132. [[CrossRef](#)]

42. Hardcastle, F.D. Raman Spectroscopy of Titania (TiO₂) Nanotubular WaterSplitting Catalysts. *J. Ark. Acad. Sci.* **2011**, *65*, 9. [[CrossRef](#)]
43. Aguilar, T.; Navas, J.; De Los Santos, D.M.; Sánchez-Coronilla, A.; Fernández-Lorenzo, C.; Alcántara, R.; Gallardo, J.J.; Blanco, G.; Martín-Calleja, J. TiO₂ and pyrochlore Tm₂Ti₂O₇ based semiconductor as a photoelectrode for dye-sensitized solar cells. *J. Phys. D Appl. Phys.* **2015**, *48*, 145102. [[CrossRef](#)]
44. Tulli, F.; Morales, J.M.N.; Salas, E.E.; Vieyra, F.E.M.; Borsarelli, C.D. Photocatalytic Efficiency Tuning by the Surface Roughness of TiO₂ Coatings on Glass Prepared by the Doctor Blade Method. *Photochem. Photobiol.* **2021**, *97*, 22–31. [[CrossRef](#)]
45. Sarker, S.; Nath, N.C.; Rahman, M.; Lim, S.S.; Ahammad, A.J.; Choi, W.Y.; Lee, J.J. TiO₂ Paste Formulation for Crack-Free Mesoporous Nanocrystalline Film of Dye-Sensitized Solar Cells. *J. Nanosci. Nanotechnol.* **2012**, *12*, 5361–5366. [[CrossRef](#)]
46. Chen, Y.; Dionysiou, D.D. Bimodal mesoporous TiO₂-P25 composite thick films with high photocatalytic activity and improved structural integrity. *Appl. Catal. B Environ.* **2008**, *80*, 147–155. [[CrossRef](#)]
47. Patrocínio, A.O.T.; Paula, L.F.; Paniago, R.M.; Freitag, J.; Bahnemann, D.W. Layer-by-Layer TiO₂/WO₃ Thin Films as Efficient Photocatalytic Self-Cleaning Surfaces. *ACS Appl. Mater. Interfaces* **2014**, *6*, 16859–16866. [[CrossRef](#)] [[PubMed](#)]
48. Kuroiwa, A.; Nomura, Y.; Ochiai, T.; Sudo, T.; Nomoto, R.; Hayakawa, T.; Kanzaki, H.; Nakamura, Y.; Hanada, N. Antibacterial, Hydrophilic Effect and Mechanical Properties of Orthodontic Resin Coated with UV-Responsive Photocatalyst. *Materials* **2018**, *11*, 889. [[CrossRef](#)]
49. Borrás, A.; López, C.; Rico, V.; Gracia, F.; González-Elipe, A.R.; Richter, E.; Battiston, G.; Gerbasi, R.; McSpornan, N.; Sauthier, G.; et al. Effect of Visible and UV Illumination on the Water Contact Angle of TiO₂ Thin Films with Incorporated Nitrogen. *J. Phys. Chem. C* **2007**, *111*, 1801–1808. [[CrossRef](#)]
50. Dulian, P.; Nachit, W.; Jaglarz, J.; Zięba, P.; Kanak, J.; Żukowski, W. Photocatalytic methylene blue degradation on multilayer transparent TiO₂ coatings. *Opt. Mater.* **2019**, *90*, 264–272. [[CrossRef](#)]
51. Lin, Y.; Qian, Q.; Chen, Z.; Dinh Tuan, P.; Feng, D. Fabrication of high specific surface area TiO₂ nanopowders by anodization of porous titanium. *Electrochem. Commun.* **2022**, *136*, 107234. [[CrossRef](#)]
52. Supphasirongjaroen, P.; Praserttham, P.; Panpranot, J.; Na-Ranong, D.; Mekasuwandumrong, O. Effect of quenching medium on photocatalytic activity of nano-TiO₂ prepared by solvothermal method. *Chem. Eng. J.* **2008**, *138*, 622–627. [[CrossRef](#)]
53. Liao, D.L.; Liao, B.Q. Shape, size and photocatalytic activity control of TiO₂ nanoparticles with surfactants. *J. Photochem. Photobiol. A Chem.* **2007**, *187*, 363–369. [[CrossRef](#)]
54. Hou, H.; Shang, M.; Wang, L.; Li, W.; Tang, B.; Yang, W. Efficient Photocatalytic Activities of TiO₂ Hollow Fibers with Mixed Phases and Mesoporous Walls. *Sci. Rep.* **2015**, *5*, 15228. [[CrossRef](#)] [[PubMed](#)]
55. Zhang, S.; Yang, D.; Jing, D.; Liu, H.; Liu, L.; Jia, Y.; Gao, M.; Guo, L.; Huo, Z. Enhanced photodynamic therapy of mixed phase TiO₂(B)/anatase nanofibers for killing of HeLa cells. *Nano Res.* **2014**, *7*, 1659–1669. [[CrossRef](#)]
56. Huang, D.; Liu, H.; Bian, J.; Li, T.; Huang, B.; Niu, Q. High Specific Surface Area TiO₂ Nanospheres for Hydrogen Production and Photocatalytic Activity. *J. Nanosci. Nanotechnol.* **2020**, *20*, 3217–3224. [[CrossRef](#)] [[PubMed](#)]
57. LI, D.; ZHANG, W. Influence of PECVD-TiO₂ film morphology and topography on the spectroscopic ellipsometry data fitting process. *Mod. Phys. Lett. B* **2020**, *34*, 2050228. [[CrossRef](#)]
58. Maeng, W.Y.; Yoon, J.H.; Kim, D.J. Effect of process conditions (withdrawal rate and coating repetition) on morphological characteristics of sol-gel TiO₂ film during dip coating. *J. Coat. Technol. Res.* **2020**, *17*, 1171–1193. [[CrossRef](#)]
59. Xiao-Hua, L.; Shu-Qin, Y.; Yu, Z.; Zhi-An, W.; Ning-Kang, H. Effects of Different Dispersion Methods on the Microscopical Morphology of TiO₂ Film. *Chin. Phys. Lett.* **2007**, *24*, 3567–3569. [[CrossRef](#)]
60. Meek, S.J.; Pitman, C.L.; Miller, A.J.M. Deducing Reaction Mechanism: A Guide for Students, Researchers, and Instructors. *J. Chem. Educ.* **2016**, *93*, 275–286. [[CrossRef](#)]
61. Gaya, U.I. *Heterogeneous Photocatalysis Using Inorganic Semiconductor Solids*; Springer Science & Business Media: Berlin/Heidelberg, Germany, 2014. [[CrossRef](#)]
62. Bogdan, J.; Zarzyńska, J.; Pławińska-Czarnak, J. Comparison of Infectious Agents Susceptibility to Photocatalytic Effects of Nanosized Titanium and Zinc Oxides: A Practical Approach. *Nanoscale Res. Lett.* **2015**, *10*, 1–15. [[CrossRef](#)]
63. Kim, B.; Kim, D.; Cho, D.; Cho, S. Bactericidal effect of TiO₂ photocatalyst on selected food-borne pathogenic bacteria. *Chemosphere* **2003**, *52*, 277–281. [[CrossRef](#)] [[PubMed](#)]
64. Jacoby, W.A.; Maness, P.C.; Wolfrum, E.J.; Blake, D.M.; Fennell, J.A. Mineralization of bacterial cell mass on a photocatalytic surface in air. *Environ. Sci. Technol.* **1998**, *32*, 2650–2653. [[CrossRef](#)]
65. Sunada, K.; Kikuchi, Y.; Hashimoto, K.; Fujishima, A. Bactericidal and detoxification effects of TiO₂ thin film photocatalysts. *Environ. Sci. Technol.* **1998**, *32*, 726–728. [[CrossRef](#)]
66. Liu, J.-W.; Chang, H.-H. Bactericidal Effects and Mechanisms of Visible Light-Responsive Titanium Dioxide Photocatalysts on Pathogenic Bacteria. *Arch. Immunol. Ther. Exp.* **2012**, *60*, 267–275. [[CrossRef](#)]
67. Yu, J.C.; Ho, W.; Yu, J.; Yip, H.; Wong, P.K.; Zhao, J. Efficient Visible-Light-Induced Photocatalytic Disinfection on Sulfur-Doped Nanocrystalline Titania. *Environ. Sci. Technol.* **2005**, *39*, 1175–1179. [[CrossRef](#)]
68. Eezzeldin, H.M.; Badi, S.; Youssef, B.A. The Antibiotic Resistance and Multidrug Resistance Pattern of Uropathogenic Escherichia coli at Soba University Hospital: A Descriptive Retrospective Survey. *Sudan J. Med. Sci.* **2022**, *17*, 56–69. [[CrossRef](#)]
69. Taba, A.; Laupland, K.B. Update on Staphylococcus aureus bacteraemia. *Curr. Opin. Crit. Care* **2022**, *28*, 495–504. [[CrossRef](#)]

70. Meyer, G.; Picoli, S.U. Fenótipos de betalactamases em *Klebsiella pneumoniae* de hospital de emergência de Porto Alegre. *J. Bras. Patol. Med. Lab.* **2011**, *47*, 24–31. [CrossRef]
71. Podgórska-Kryszczuk, I.; Solarska, E.; Kordowska-Wiater, M. Reduction of the Fusarium Mycotoxins: Deoxynivalenol, Nivalenol and Zearalenone by Selected Non-Conventional Yeast Strains in Wheat Grains and Bread. *Molecules* **2022**, *27*, 1578. [CrossRef]
72. Long, H.; Pu, L.; Xu, W.; Nan, M.; Oyom, W.; Prusky, D.; Bi, Y.; Xue, H. Inactivation of *Penicillium expansum* spores in apple juice by contact glow discharge electrolysis and its related mechanism. *Innov. Food Sci. Emerg. Technol.* **2022**, *80*, 103100. [CrossRef]
73. Golshan, V.; Mirjalili, F.; Fakharpour, M. Self-Cleaning Surfaces with Superhydrophobicity of Ag–TiO₂ Nanofilms on the Floor Ceramic Tiles. *Glass Phys. Chem.* **2022**, *48*, 35–42. [CrossRef]
74. Kisand, V.; Visnapuu, M.; Rosenberg, M.; Danilian, D.; Vlassov, S.; Kook, M.; Lange, S.; Pärna, R.; Ivask, A. Antimicrobial Activity of Commercial Photocatalytic SaniTise™ Window Glass. *Catalysts* **2022**, *12*, 197. [CrossRef]
75. Hegyi, A.; Grebenisan, E.; Lazarescu, A.-V.; Stoian, V.; Szilagyi, H. Influence of TiO₂ Nanoparticles on the Resistance of Cementitious Composite Materials to the Action of Fungal Species. *Materials* **2021**, *14*, 4442. [CrossRef]
76. Foster, H.A.; Sheel, D.W.; Sheel, P.; Evans, P.; Varghese, S.; Rutschke, N.; Yates, H.M. Antimicrobial activity of titania/silver and titania/copper films prepared by CVD. *J. Photochem. Photobiol. A Chem.* **2010**, *216*, 283–289. [CrossRef]
77. Ditta, I.B.; Steele, A.; Liptrot, C.; Tobin, J.; Tyler, H.; Yates, H.M.; Sheel, D.W.; Foster, H.A. Photocatalytic antimicrobial activity of thin surface films of TiO₂, CuO and TiO₂/CuO dual layers on *Escherichia coli* and bacteriophage T4. *Appl. Microbiol. Biotechnol.* **2008**, *79*, 127–133. [CrossRef]
78. Evans, P.; Sheel, D.W. Photoactive and antibacterial TiO₂ thin films on stainless steel. *Surf. Coat. Technol.* **2007**, *201*, 9319–9324. [CrossRef]
79. ISO 10678:2010; Fine Ceramics (Advanced Ceramics, Advanced Technical Ceramics): Determination of Photocatalytic Activity of Surfaces in an Aqueous Medium by Degradation of Methylene Blue. International Organization for Standardization ISO: Geneva, Switzerland, 2010. Available online: <https://www.iso.org/standard/46019.html> (accessed on 15 March 2023).

Disclaimer/Publisher's Note: The statements, opinions and data contained in all publications are solely those of the individual author(s) and contributor(s) and not of MDPI and/or the editor(s). MDPI and/or the editor(s) disclaim responsibility for any injury to people or property resulting from any ideas, methods, instructions or products referred to in the content.